




## Energy absorption of AlSi10Mg origami cellular structures fabricated via laser powder bed fusion

**Hiromi Yasuda** , Institute of Space and Astronautical Science, Japan Aerospace Exploration Agency, Sagamihara, Kanagawa 252-5210, Japan; Aviation Technology Directorate, Japan Aerospace Exploration Agency, Mitaka, Tokyo 181-0015, Japan  
**Takahiro Kunimine**, Faculty of Mechanical Engineering, Institute of Science and Engineering, Kanazawa University, Kakuma-machi, Kanazawa, Ishikawa 920-1192, Japan

Address all correspondence to Hiromi Yasuda at [yasuda.hiromi@jaxa.jp](mailto:yasuda.hiromi@jaxa.jp)

(Received 1 December 2023; accepted 12 January 2024)

### Abstract

We experimentally study the energy absorption of metallic origami cellular structures additively manufactured from an AlSi10Mg alloy. We fabricate AlSi10Mg origami using the laser powder bed fusion (L-PBF) process. Since the as-fabricated AlSi10Mg has limited elongation at break, we systematically examine the heat treatment conditions and achieve the large deformation (i.e., wide folding range) of AlSi10Mg origami without fracture of origami creases. In addition, we use a drop tower impact system to demonstrate the effectiveness of AlSi10Mg origami's folding behavior for impact energy absorption. Based on our experimental results, AlSi10Mg origami cellular structures could be exploited to develop a highly efficient lightweight impact absorber.

### Introduction

Thin-walled structures are used in a wide range of engineering fields due to their enhanced mechanical performance, such as lightweight design,<sup>[1]</sup> impact energy absorption,<sup>[2-4]</sup> and tunable stiffness.<sup>[5]</sup> Origami provides an ideal platform to construct such architecture through folding thin sheets (i.e., making crease lines). The design strategy based on origami can offer not only 2D planar structures (e.g., Miura-ori<sup>[6]</sup>) but also 3D volumetric systems (e.g., cellular materials consisting of origami tubes<sup>[7]</sup>). However, the geometry of 3D origami architectures tends to be complex, causing manufacturing challenges, especially fabrication from sheet materials.

In recent decades, additive manufacturing (AM) technologies have been developed rapidly, enabling the fabrication of architected materials with complex geometries, including cellular lattice structures.<sup>[8]</sup> In particular, metallic additive manufacturing has been exploited recently for industrial products ranging from medical devices to aerospace structural elements.<sup>[9-11]</sup> One commonly used approach for metallic AM is laser powder bed fusion (L-PBF), also known as selective laser melting (SLM). Recently, origami-based cellular structures, specifically stacked Miura-ori cellular materials, have been fabricated from stainless steel 316 L via the L-PBF process, exhibiting the effectiveness of metallic additively manufactured origami structures for large deformation (i.e., folding motion), particularly energy absorption behavior.<sup>[12,13]</sup>

Here, we experimentally demonstrate the efficient energy absorption of a lightweight metallic origami cellular material fabricated from aluminum alloys, specifically AlSi10Mg (Fig. 1). Since the density ( $\rho$ ) of AlSi10Mg is typically  $2670 \text{ kg/m}^3$ , it is advantageous to design a lightweight cellular

structure using Al alloys compared to stainless steel materials ( $\rho = 7900 \text{ kg/m}^3$ ). However, it has been shown that the as-fabricated L-PBF AlSi10Mg alloys exhibit lower elongation at break (6.3% for AlSi10Mg,<sup>[14]</sup> whereas more than 40% for stainless steel 316 L,<sup>[15]</sup>) which limits the folding motion of origami structures. Previous studies have reported enhancing the mechanical properties of L-PBF-processed AlSi10Mg alloys via subsequent heat treatment (e.g.,<sup>[16]</sup>). In the present study, we systematically examine the effect of heat treatments, especially heat treatment temperatures, by performing tensile coupon tests and compression tests on the cellular origami structures. In addition, we introduce variable thickness for face and crease parts to enhance the folding motion of AlSi10Mg origami, which has been unexplored previously for metallic origami. We then demonstrate the impact-absorbing behavior that relies on the rigid origami folding motion by applying dynamic impact to the AlSi10Mg prototypes.

### Materials and methods

#### Design and fabrication of AlSi10Mg origami

We start by designing the geometry of origami cellular structures, specifically the Tachi-Miura polyhedron (TMP)<sup>[17-19]</sup> [Fig. 1(a)]. The TMP is a bellows-like origami that shows a rigid origami folding motion in which the deformation takes only along the crease lines [see Fig. 1(b)]. Previous studies on the TMP have shown rich physical properties, such as load-bearing capability,<sup>[20]</sup> high reconfigurability,<sup>[21]</sup> and efficient impact energy absorption.<sup>[22]</sup> Note that the TMP structures have been fabricated mainly from paper sheets or soft materials in

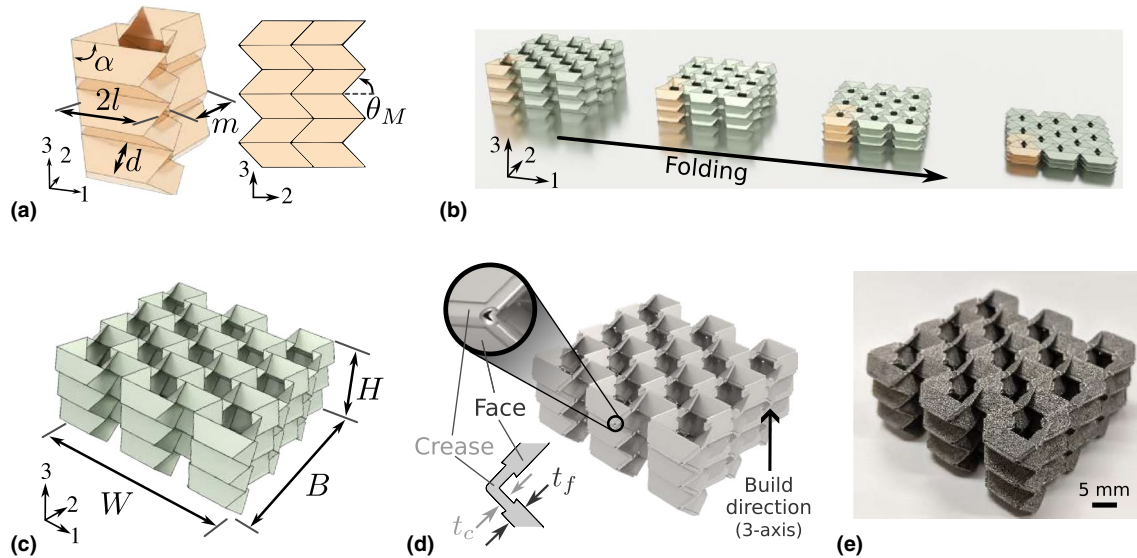


**Figure 1.** Geometry of the Tachi-Miura Polyhedron (TMP). (a) The unit cell geometry of the TMP. The length parameters ( $l, m, d$ ), angle parameter ( $\alpha$ ), and the folding angle ( $\theta_M$ ) are illustrated in (Left) the 3D view and (Right) side view. (b) The folding motion of the  $5 \times 3$  origami cellular structure. Three different models of the  $5 \times 3$  TMP tessellation; (c) Zero thickness origami model, (d) origami with non-zero thickness, and (e) additively manufactured AISi10Mg origami prototype.

the previous work, and the fabrication of the TMP from metallic materials has been unexplored. The unit cell geometry can be defined by the length parameters ( $l, m, d$ ) and the angle ( $\alpha$ ) between the horizontal and inclined creases [see the left illustration of Fig. 1(a)]. To define the folded configuration, we introduce the folding angle  $\theta_M$ , which is a half angle of the horizontal crease line [see the side view of the TMP unit cell shown in Fig. 1(a)]. Then, a cellular configuration composed of multiple TMP unit cells can be designed [see Fig. 1(b) for the folding motion of the TMP tessellation]. Here, the width ( $W$ ), breadth ( $B$ ), and height ( $H$ ) of the (zero thickness) rigid origami cellular structure can be calculated as follows [Fig. 1(c)]:

$$W = 2N_1l + \frac{d}{\tan \alpha} + \beta m \cos \theta_G, \quad (1)$$

$$B = 2N_2m \sin \theta_G + d \cos \theta_M, \quad (2)$$

$$H = N_3d \sin \theta_M, \quad (3)$$

where  $N_3$  is the number of layers in the 3-axis and  $N_1$  and  $N_2$  are the numbers of TMP unit cells in the 1- and 2-axes, respectively. Also,

$$\tan \left( \frac{\theta_G}{2} \right) = \tan \alpha \cos \theta_M, \quad (4)$$

$$\beta = \begin{cases} N_1 + 1, & \text{if } \cos \theta_M \leq 1/\tan \alpha, \\ N_1 - 1, & \text{otherwise.} \end{cases} \quad (5)$$

Based on the rigid origami model [Fig. 1(c)], we add thickness to each surface of the origami to build the origami structure with non-zero thickness [Fig. 1(d)] for additive manufacturing. Note that we use two different thickness values ( $t_f$  and  $t_c$ ) for

the face and crease parts to enhance the folding motion under compression [see the inset of Fig. 1(d)]. In this study,  $t_f = 0.6$  mm and  $t_c = 0.4$  mm are used.

Finally, we fabricate the (non-zero thickness) origami cellular structure via L-PBF. We use the EOS M290 system to additively manufacture origami cellular structures from AISi10Mg [Fig. 1(e)]. After the L-PBF process, we consider the various heat treatment conditions to enhance the folding motion of the origami structure under compression, particularly the deformation around the creases. We discuss this heat treatment in the next section.

### Heat treatment condition

To enhance the folding behavior of the additively manufactured origami, we first examine the mechanical properties of AISi10Mg using tensile coupons. In particular, we focus on tensile elongation after various heat treatments [see Fig. 2(a) for the fracture points for different heat-treated coupons; also see Supplementary Movie S1]. The previous research on the additively manufactured specimens made of AISi10Mg shows that with the application of the heat treatment (e.g., 300°C for 2 h) to the as-fabricated specimens, mechanical properties such as elongation and strength can be drastically changed.<sup>[16]</sup> We consider the following five different temperatures for the heat treatment as well as the as-fabricated samples: 200°C, 250°C, 300°C, 400°C, and 500°C. Note that we apply the heat treatments at those temperatures for 2 h. For each condition, we fabricate three (rectangular) tensile coupons with a gauge length of 25 mm, a width of 6 mm, and a thickness of 3 mm based on ASTM B557 (subsize specimen). Also, the tensile direction is parallel to the building direction [see the inset image of Fig. 2(b)].

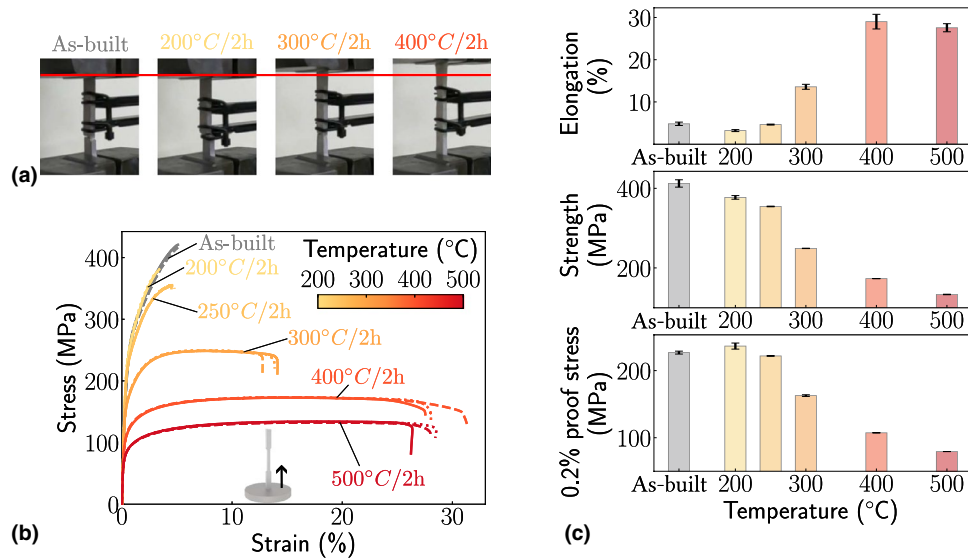


**Figure 2.** Tensile tests on coupons with a rectangular cross-section. (a) Photographs of tensile coupons at the fracture point for four different heat treatment conditions; As-built, 200°C, 300°C, and 400°C for 2 h. (b) Stress–strain curves for tensile coupons with different heat treatment temperatures. For each heat treatment condition, three specimens are tested and each result is denoted as solid, dashed, and dotted lines in the plot. (c) The tensile properties obtained from the stress–strain curves. (Upper) Elongation at break, (Middle) strength, and (Lower) 0.2 % proof stress are plotted.

Figure 2(b) shows the stress–strain curves obtained from the tensile tests performed at room temperature. In this figure, the colors indicate the heat treatment temperature, and the solid, dashed, and dotted lines denote the results of three different samples. Our tensile tests show that as we increase the temperature value, the total elongation increases significantly, especially above 250°C (for 2 h). However, the strength becomes lower for higher heat treatment temperature conditions. To examine the differences among various conditions, we extract and compare the elongation, strength, and 0.2% proof stress values in Fig. 2(c). The upper plot shows that the elongation of the as-built coupons is about 5 %; the cases of 400°C and 500°C achieve more than 20 % elongation. The strength and 0.2% proof stress values change drastically between 250°C and 300°C cases, as shown in the middle and lower plots, respectively.

This drastic change in mechanical properties arises from the microstructure change of L-PBF AlSi10Mg via heat treatment. It has been reported that due to the melt pools developed through the L-PBF process (i.e., rapid local melting and solidification), columnar  $\alpha$ -Al grains with a fine substructure consisting of tangled dislocations are formed in the as-fabricated AlSi10Mg samples,<sup>[16]</sup> which generally leads to higher strength. The application of the heat treatment (especially at over 300°C) can cause the annihilation of such fine substructures, and the mechanical properties of AlSi10Mg change accordingly (particularly reducing strength). Also, it should be noted that the as-fabricated AlSi10Mg specimens exhibit different elongation behavior depending on tensile directions (i.e., parallel/normal to the building direction) due to the presence of

the melt pool boundaries, whereas AlSi10Mg with higher heat treatment temperature (e.g., 500°C) exhibits weak anisotropy in elongation. This is because the melt pool boundaries can be removed by the heat treatment at higher temperatures.<sup>[16]</sup> Therefore, to design and fabricate AlSi10Mg origami for engineering applications requiring large deformation, we need to choose the heat treatment conditions carefully.

### Static compression test

To characterize the folding behavior of AlSi10Mg origami, we conduct the quasi-static compression test. We use the Instron 5882 universal testing machine to compress the AlSi10Mg prototypes. We fabricate 5×3 multi-cell origami structures comprising the TMP unit cells with  $(l, m, d, \alpha) = (5 \text{ mm}, 8 \text{ mm}, 5 \text{ mm}, 63^\circ)$ . Also, the folding angle  $\theta_M = 48^\circ$  is used to design the origami model with non-zero thickness [Fig. 1(e)]. Here, six prototypes are fabricated for different heat treatment conditions discussed in the previous section. We apply the compression to the AlSi10Mg origami prototype at the displacement rate of 0.1 mm/min.

### Drop tower impact test

Based on the static compression test, the drop tower impact testing is performed to analyze the energy absorption behavior of AlSi10Mg origami under dynamic impact in the 3-axis. We use the Instron Ceast 9350 drop tower impact system to characterize the dynamic response of the prototype. Also, we employ a high-speed camera (Photron FASTCAM SA-X) to capture the dynamic folding motion. The design parameters of 5×3 multi-cell origami structures are  $l = 6 \text{ mm}$  and  $\theta_M = 46^\circ$ ,

and the other parameters are identical to those in the static compression test. In this configuration, the bounding dimensions calculated numerically from the computer-aided-design (CAD) software are  $(W, B, H) = (53.0 \text{ mm}, 49.6 \text{ mm}, 22.0 \text{ mm})$ , and the volume of origami with non-zero thickness is  $7063 \text{ mm}^3$ . Based on the 3D CAD model (see Fig. 1(d)), the relative density of this origami structure is 0.12. For reference purposes, we also fabricate AlSi10Mg  $5 \times 7$  hexagonal honeycomb structures by choosing a side length of 5.15 mm and a wall thickness of 0.55 mm so that the relative density and volume are identical to those of the origami structure. Here,  $(W, B, H) = (45.1 \text{ mm}, 57.1 \text{ mm}, 21.6 \text{ mm})$ , and the volume calculated from the CAD is  $7063 \text{ mm}^3$ . The heat treatment condition for AlSi10Mg origami and honeycomb structures is  $500^\circ\text{C}$  for 2 h.

## Results and discussion

### Force–displacement relationships

We study the folding behavior of AlSi10Mg origami under quasi-static compression in three different directions (i.e., 1-, 2-, and 3-axes). Figure 3(a) shows the snapshots of the compression test for the 3-axis case. We observe that the AlSi10Mg origami shows the rigid origami-like folding motion [see

Fig. 1(b) for the rigid origami motion of the TMP], which means that deformation occurs mostly along the crease parts. During the compression test, origami prototypes with different heat treatment temperatures show a similar folding motion at the early stage of compression (see Supplementary Movie S2). However, the prototypes with lower heat treatment temperature cases show the fracture of the crease regions (see the inset image i) in Fig. 3(a) for the as-built AlSi10Mg origami after compression in the 3-axis). For the higher heat treatment temperature cases, the folding motion can be achieved without noticeable breakage of the structure (e.g., see the inset ii) in Fig. 3(a) for  $500^\circ\text{C}/2 \text{ h}$  case). Figure 3(b) shows the force–displacement relationships (compression in the 3-axis) for various heat treatment conditions. We observe the periodic fluctuation after the initial peak for the lower heat treatment temperature cases ( $200^\circ\text{C}/2 \text{ h}$  and  $250^\circ\text{C}/2 \text{ h}$ ) as well as the as-built prototype [e.g., the gray line in Fig. 3(b) for the as-built case], which is due to the layer-by-layer fractures of the crease parts. On the other hand, the higher heat treatment temperature cases ( $300^\circ\text{C}$ ,  $400^\circ\text{C}$ , and  $500^\circ\text{C}$ ) indicate a smooth evolution of the force without spikes. In addition, we observe evidently the formation of plateau regions (i.e., constant force stage) without fluctuation, which is extremely useful for energy absorption, followed by the (final) densification stage. Since the AlSi10Mg origami

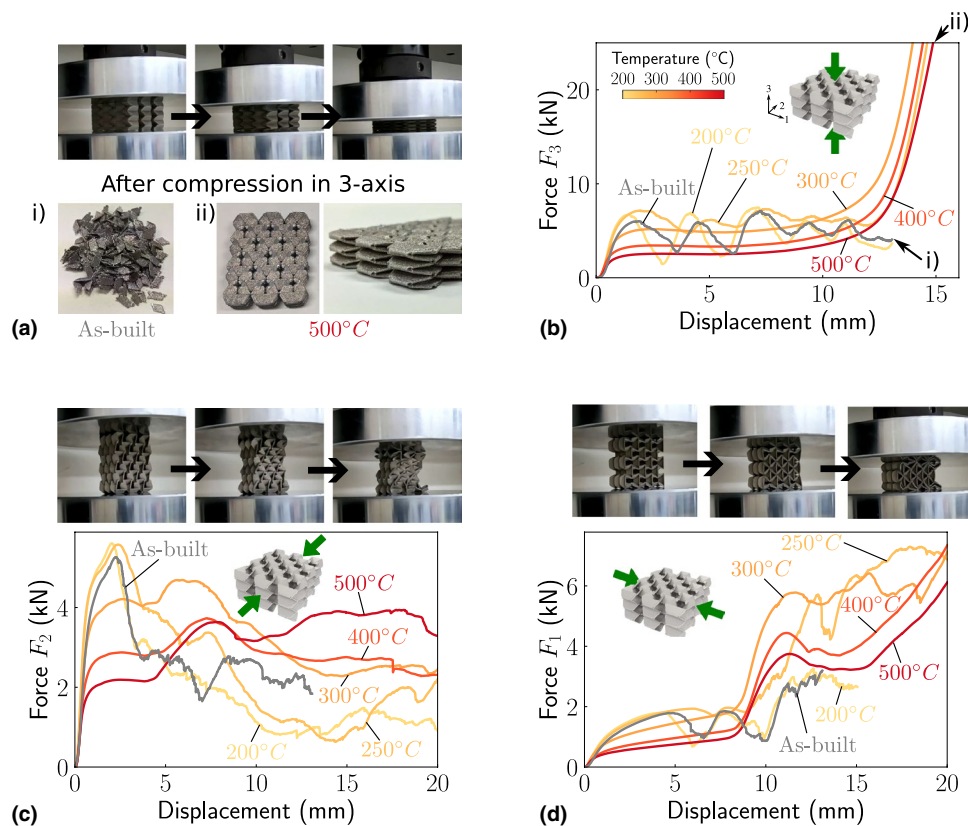


**Figure 3.** (Quasi) static compression test. (a) (Upper) Photographs showing the folding motion of the AlSi10Mg origami compressed in 3-axis. (Lower) Origami configurations after quasi-static compression for two heat treatment conditions: (i) As-built and (ii)  $500^\circ\text{C}/2 \text{ h}$ . (b) Force–displacement relationships for compression in the 3-axis are shown. The color indicates the heat treatment temperature. Also, we conduct compression tests for (c) 2-axis and (d) 1-axis.

with the heat treatment temperature of 300°C (or higher) can achieve a smooth force–displacement curve without fracture, the elongation of around 10 % (or more) is required to obtain the (smooth) rigid origami folding motion for the design parameters chosen in this study, based on the tensile coupon tests as shown in Fig. 2. Note that AlSi10Mg origami can exhibit drastically different deformation modes, i.e., brittle compressive behavior or smooth folding motion with a flat plateau region, depending on the heat treatment condition, which is different from stainless steel origami structures.

We also examine the compression in the other directions. Figures 3(c) and (d) show the compression test results for the 2- and 1-axis cases, respectively (see also Supplementary Movies 3 and 4). Although the smooth (origami-like) folding motions are observed at the beginning of the compression, the later part of the force curves shows the fluctuation triggered by the contact between neighboring faces (or vertices). This is because the range of the rigid folding motion is limited if we apply the compression in the 1-/2-axis.

### Energy absorption under impact

Based on the static compression tests, we investigate the dynamic folding behavior of the AlSi10Mg origami for energy absorption, specifically the crush response in the 3-axis. Figure 4(a) shows snapshots of the drop tower impact testing on the origami structure (see the upper row) and the honeycomb structure (lower row) (see also Supplementary Movie S5). Here, we apply the impact energy of 27.8 J, corresponding to the impactor speed of 2.51 m/s. The high-speed camera images show a rigid-origami-like folding motion similar to the static compression test result [Fig. 3(a)]. For the honeycomb with

the same relative density as the origami, the impactor bounces back immediately after the impactor and honeycomb are in contact [see the red line in Fig. 4(a)]. Figure 4(b) shows the force profiles for the origami (red line) and honeycomb (gray) cases as a function of time. Remarkably, the origami structure exhibits an extremely lower force level and longer contact time than the honeycomb case, in which a sharp initial force peak is observed (see Supplementary Movies S6 and S7).

To analyze the energy absorption of the origami from the folding motion, we compare static and impact test results in terms of the energy from the deformation under quasi-static compression or dynamic impact. By using the force–displacement curve from the static compression test [the upper plot in Fig. 4(c)], we calculate the energy  $W$  defined as

$$W(u_3) = \int_0^{u_3} F_3 du, \quad (6)$$

where  $u_3$  represents the deformation in the 3-axis. In the lower panel of Fig. 4(c), we plot the calculated energy curve (red line) and the impact test results (green markers). For the impact test results, we measure the deformation (i.e., height change) of each origami after dynamic impact for three different impact energy cases: 14.8 J (the corresponding impact speed is 1.83 m/s), 26.1 J (2.43 m/s), and 27.8 J (2.51 m/s). Our analysis indicates reasonably good agreement between the impact test results and the energy values calculated from the static compression test, which means that the impact energy is efficiently absorbed by the origami deformation (i.e., the folding motion). Therefore, the AlSi10Mg origami structure can be useful for engineering applications such as efficient impact absorbers, especially for low-velocity impact mitigation.

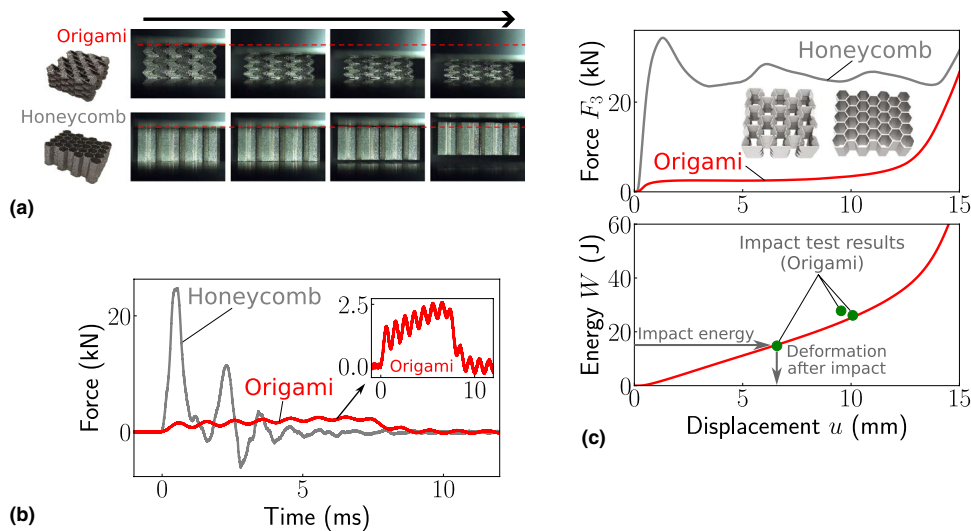


**Figure 4.** Drop tower impact testing. (a) High-speed camera images show the compressive behaviors of the origami and honeycomb under the impact (the impact energy is 27.8 J for both cases). (b) The force profiles measured from the impact testing for origami (red solid line) and honeycomb (gray) are shown. The inset shows the magnified plot for the origami case. (c) (Upper) Force–displacement curves for the origami with  $l = 6$  mm (red line) and honeycomb lattice (gray) obtained from the static compression test. The relative density of both origami and honeycomb structures is 0.12. Based on the force–displacement curves, the calculated energy curve for origami is shown (Lower). The green markers indicate the impact testing results for origami (Color figure online).

## Conclusion

We have studied the static and dynamic folding behavior of the metallic additively manufactured origami cellular structures fabricated via laser powder bed fusion (L-PBF). The origami cellular structure is composed of the Tachi-Miura polyhedron (TMP) unit cells with non-zero thickness. We have fabricated origami structures using AlSi10Mg and examined various heat treatment conditions after the L-PBF process to enhance the origami folding motions. We have conducted the quasi-static compression test to characterize the static response of our origami prototypes, and our experimental results show that AlSi10Mg origami can exhibit drastically different static responses depending on the heat treatment conditions (i.e., collapse mode with layer-by-layer crease fractures and a well-controlled force–displacement curve with a wide plateau region), especially for the compression in the 3-axis. In addition, we have experimentally demonstrated the effective energy absorption of the AlSi10Mg origami for several impact cases by using the drop tower impact system. Although this study focused on low-velocity impact, we envision that the AlSi10Mg origami can be developed for different impact ranges by optimizing the energy absorption efficiency (e.g., altering geometric parameters to tailor the force–displacement relation or changing the heat treatment condition to enhance the strength of AlSi10Mg alloys). Moreover, by leveraging the additive manufacturing technique, one can select different metallic (or soft) materials (e.g., steel, titanium, etc.) to fabricate the origami cellular structure for various purposes. Therefore, the metallic origami cellular structure, together with additive manufacturing, has great potential to develop novel engineering devices such as lightweight cellular structures for power plants and efficient impact absorbers for aerospace applications.

## Acknowledgments

We thank NTT Data XAM Technologies and Masanori Sakaino of Japan Aerospace Exploration Agency for prototype fabrication. We also thank Takashi Yamazaki of Kiguchi Technics Inc. and Hiromitsu Miyaki of Japan Aerospace Exploration Agency for technical support. H.Y. and T.K. are grateful for the support from JSPS KAKENHI Grant-in-Aid for Challenging Research (Exploratory) 22K18750.

## Author contributions

HY and TK conceived the research topic. HY conducted the design and testing of prototypes. HY and TK contributed to writing and editing the manuscript.

## Funding

This work was supported by JSPS KAKENHI Grant-in-Aid for Challenging Research (Exploratory) 22K18750.

## Data availability

The datasets are available from the corresponding author on reasonable request.

## Declarations

## Conflict of interest

The authors declare no conflict of interest.

## Supplementary Information

The online version contains supplementary material available at <https://doi.org/10.1557/s43579-024-00518-7>.

## Open Access

This article is licensed under a Creative Commons Attribution 4.0 International License, which permits use, sharing, adaptation, distribution and reproduction in any medium or format, as long as you give appropriate credit to the original author(s) and the source, provide a link to the Creative Commons licence, and indicate if changes were made. The images or other third party material in this article are included in the article's Creative Commons licence, unless indicated otherwise in a credit line to the material. If material is not included in the article's Creative Commons licence and your intended use is not permitted by statutory regulation or exceeds the permitted use, you will need to obtain permission directly from the copyright holder. To view a copy of this licence, visit <http://creativecommons.org/licenses/by/4.0/>.

## References

1. L.J. Gibson, M.F. Ashby, *Cellular solids: structure and properties*. Cambridge solid state science series, 2nd edn. (Cambridge University Press, Cambridge, 1997). <https://doi.org/10.1017/CBO9781139878326>
2. W. Abramowicz, N. Jones, Dynamic progressive buckling of circular and square tubes. *Int. J. Impact Eng* **4**(4), 243–270 (1986)
3. J. Ma, Z. You, Energy absorption of thin-walled square tubes with a prefolded origami pattern-part I: geometry and numerical simulation. *J. Appl. Mech.* **81**(1), 011003 (2013). <https://doi.org/10.1115/1.4024405>
4. C. Zhou, B. Wang, J. Ma, Z. You, Dynamic axial crushing of origami crash boxes. *Int. J. Mech. Sci.* **118**, 1–12 (2016). <https://doi.org/10.1016/j.ijmecsci.2016.09.001>
5. X. Yu, J. Zhou, H. Liang, Z. Jiang, L. Wu, Mechanical metamaterials associated with stiffness, rigidity and compressibility: a brief review. *Prog. Mater. Sci.* **94**, 114–173 (2018). <https://doi.org/10.1016/j.pmatsci.2017.12.003>
6. K. Miura, Method of packaging and deployment of large membranes in space. The Institute of Space and Astronautical Science Report No. 618, 1–9 (1985)
7. E.T. Filipov, T. Tachi, G.H. Paulino, Origami tubes assembled into stiff, yet reconfigurable structures and metamaterials. *Proc. Natl. Acad. Sci. USA* **112**, 12321–12326 (2015). <https://doi.org/10.1073/pnas.1509465112>
8. X. Zheng, H. Lee, T.H. Weisgraber, M. Shusteff, J. DeOtte, E.B. Duoss, J.D. Kuntz, M.M. Biener, Q. Ge, J.A. Jackson, S.O. Kucheyev, N.X. Fang, C.M. Spadaccini, Ultralight, ultrastiff mechanical metamaterials. *Science* **344**(6190), 1373–1377 (2014)

9. C. Culmone, G. Smit, P. Breedveld, Additive manufacturing of medical instruments: a state-of-the-art review. *Addit. Manuf.* **27**, 461–473 (2019)
10. K. Chua, I. Khan, R. Malhotra, D. Zhu, Additive manufacturing and 3D printing of metallic biomaterials. *Eng. Regen.* **2**, 288–299 (2021)
11. B. Blakey-Milner, P. Gradl, G. Snedden, M. Brooks, J. Pitot, E. Lope, M. Leary, F. Berto, A. Plessis, Metal additive manufacturing in aerospace: a review. *Mater. Des.* **209**, 110008 (2021)
12. J.A. Harris, G.J. McShane, Metallic stacked origami cellular materials: additive manufacturing, properties, and modelling. *Int. J. Solids Struct.* **185–186**, 448–466 (2020). <https://doi.org/10.1016/j.ijsolstr.2019.09.007>
13. J.A. Harris, G.J. McShane, Impact response of metallic stacked origami cellular materials. *Int. J. Impact Eng.* **147**, 103730 (2021). <https://doi.org/10.1016/j.ijimpeng.2020.103730>
14. EOS Aluminium AlSi10Mg Material Data Sheet. [https://www.eos.info/03\\_system-related-assets/material-related-contents/metal-materials-and-examples/metal-material-datasheet/aluminium/material\\_datasheet\\_eos\\_aluminium-alsi10mg\\_en\\_web.pdf](https://www.eos.info/03_system-related-assets/material-related-contents/metal-materials-and-examples/metal-material-datasheet/aluminium/material_datasheet_eos_aluminium-alsi10mg_en_web.pdf) Accessed 25 Nov 2023
15. EOS StainlessSteel 316L Material Data Sheet. [https://www.eos.info/03\\_system-related-assets/material-related-contents/metal-materials-and-examples/metal-material-datasheet/stainlesssteel/material\\_datasheet\\_eos\\_stainlesssteel\\_316l\\_en\\_web.pdf](https://www.eos.info/03_system-related-assets/material-related-contents/metal-materials-and-examples/metal-material-datasheet/stainlesssteel/material_datasheet_eos_stainlesssteel_316l_en_web.pdf) Accessed 25 Nov 2023
16. N. Takata, H. Kodaira, K. Sekizawa, A. Suzuki, M. Kobashi, Change in microstructure of selectively laser melted AlSi10Mg alloy with heat treatments. *Mater. Sci. Eng. A* **704**, 218–228 (2017)
17. K. Miura, T. Tachi, Synthesis of rigid-foldable cylindrical polyhedra. *J. Int. Soc. Interdiscip. Study Symmetry* **2010**, 204–213 (2010)
18. T. Tachi, K. Miura, Rigid-foldable cylinders and cells. *J. Int. Assoc. Shell Spatial Struct.* **53**, 217–226 (2012)
19. H. Yasuda, J. Yang, Reentrant origami-based metamaterials with negative Poisson's ratio and bistability. *Phys. Rev. Lett.* **114**(18), 185502 (2015). <https://doi.org/10.1103/PhysRevLett.114.185502>
20. H. Yasuda, B. Gopalarethinam, T. Kunimine, T. Tachi, J. Yang, Origami-based cellular structures with in situ transition between collapsible and load-bearing configurations. *Adv. Eng. Mater.* **21**, 1900562 (2019). <https://doi.org/10.1002/adem.201900562>
21. Y. Miyazawa, H. Yasuda, H. Kim, J.H. Lynch, K. Tsujikawa, T. Kunimine, J.R. Raney, J. Yang, Heterogeneous origami-architected materials with variable stiffness. *Commun. Mater.* **2**, 110 (2021). <https://doi.org/10.1038/s43246-021-00212-4>
22. S. Tomita, K. Shimanuki, H. Nishigaki, S. Oyama, T. Sasagawa, D. Murai, K. Umamoto, Origami-inspired metamaterials with switchable energy absorption based on bifurcated motions of a Tachi-Miura polyhedron. *Mater. Des.* **225**, 111497 (2023). <https://doi.org/10.1016/j.matdes.2022.111497>

**Publisher's Note** Springer Nature remains neutral with regard to jurisdictional claims in published maps and institutional affiliations.